

1A.1 Preliminary Results from the Multi-Angle Snowflake and Radar (MASCRA) Project.

Patrick C. Kennedy^{a1} C. Kleinkort^a, G. J. Huang^a, M. Thurai^a, A. Newman^b,

J. C. Hubbert^b, S. Rutledge^a, V. N. Bringi^a, and B. Notaroš^a

^a Colorado State University, Fort Collins, Colorado

^b NCAR, Boulder, Colorado

1. INTRODUCTION

The Multi-Angle Snowflake and Radar Project (MASCRA) is designed to collect ground-level snow particle image data from which detailed three dimensional reconstructions of the hydrometeors can be prepared. These 3D representations of the particle's ice / air structures provide input specifications for advanced microwave scattering formulations (Chobanyn et al., 2015). Dual-polarization data collected by the CSU-CHILL and NCAR S-Pol radars is used to check the fidelity of these scattering calculations. The details of the 3D reconstruction procedures and associated microwave scattering results are presented in Kleinkort et al. (2015). This paper deals with instrumentation used to obtain the hydrometeor images and presents selected particle images and radar data collected during three MASCRA cases with widely-differing meteorological settings during the project's initial operational period (November 2014 – April 2015).

To reduce the vertical separation between the radar sample volume and the surface-based measurements, a search was undertaken to locate an instrumentation site within 15 km of the CSU-CHILL radar (located near Greeley, Colorado). The selected location was on the property of the Easton – Valley View airport at azimuth 171.3° / range 13.03 km from CSU-CHILL. The ground elevation at the Easton Airport is ~32 m higher than the terrain height at CSU-CHILL. Due to ground clutter, the lowest elevation angle at which uncontaminated meteorological data can be collected with the CSU-CHILL S-band system in the immediate Easton vicinity is 1.5°. At this elevation angle, the antenna pattern's main lobe is located between the ~192 and 420 m heights above the ground at the Easton Airport site. An overview of the location of the Easton Airport site with respect to the CSU-CHILL and NCAR S-Pol radars is shown in Figure 1. When precipitation was occurring or expected at Easton, both CSU-CHILL and S-Pol conducted pre-programmed, ~4 minute cycle time scan sequences that included both low-elevation

angle PPI's as well as narrow RHI volumes centered on the ground instrumentation site.

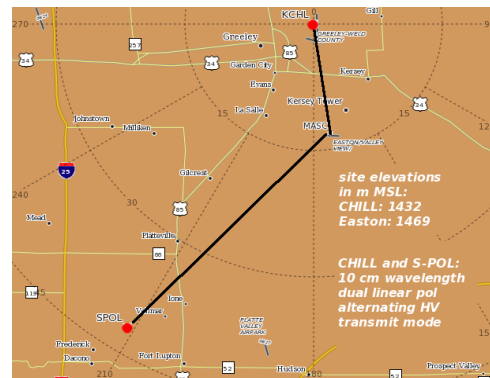


Figure 1: Locations of the CSU-CHILL and NCAR S-Pol radars with respect to the Easton Airport surface instrumentation site.

A 2/3's scale (8 m outer diameter) Double Fence Intercomparison Reference (DFIR) wind screen was constructed at the Easton site to reduce the impacts of horizontal wind on the collection efficiency of the hydrometeor sensors. Figure 2 shows the arrangement of the instruments located inside the wind screen.



Figure 2: Instrumentation installed at the Easton Airport site during the November 2014 – April 2015 period of MASCRA project operations.

¹ Corresponding Author: Patrick.Kennedy@colostate.edu

Conventional precipitation accumulation measurements vs. time were obtained using an OTT Pluvio weighing-type gauge. Mesonet sensors provided by NCAR measured atmospheric state variables and surface winds at locations both inside and outside of the DFIR wind screen. NCAR also installed an MGAUS mobile sounding system to allow the launching of radiosondes from the Easton site during periods of intensive observations.

2. The MASC and 2DVD instruments

Individual hydrometeor shape and size information was provided by the Multi-Angle Snowflake Camera (MASC) and by the two dimensional video disdrometer (2DVD). The basic MASC design obtains snow particle images using three digital cameras installed in a common horizontal plane (Garrett et al, 2012). Figure 3 shows an overview of the camera and flash illumination arrangement. The irregularly-shaped yellow planes shown in this figure depict the beams of the two vertically-separated IR beams; the interruption of these beams triggers both the flash units and the cameras. The time difference between the interruptions of the individual beams is used to calculate a fall speed value.

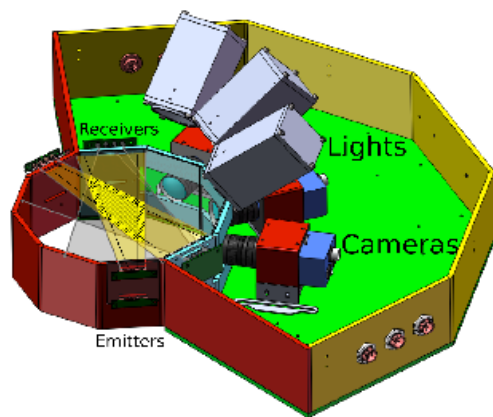


Figure 3: MASC schematic diagram. (From Garrett et al, 2012).

The CSU MASC uses three Unibrain 980 digital cameras. Each camera produces 5 Mpixel image files with resolutions as small as 50 μm . To facilitate the 3D image reconstruction process, two additional lower resolution cameras (1.2 Mpixel Unibrain 785) with a downward-looking viewing angle were added (Fig. 4).



Figure 4: Two additional downward-looking cameras added to the CSU MASC.

In contrast to the black and white digital photographic images captured by the individual MASC cameras, the two dimensional video disdrometer (2DVD) sequentially records the shadowing that occurs across a linear array of 160 μm resolution photodiodes as hydrometeors fall through a horizontal plane of visible light (Schönhuber, 2008). Two light source / line scan cameras with perpendicular viewing directions are used to obtain orthogonal silhouette views of the particle (Fig. 5a)

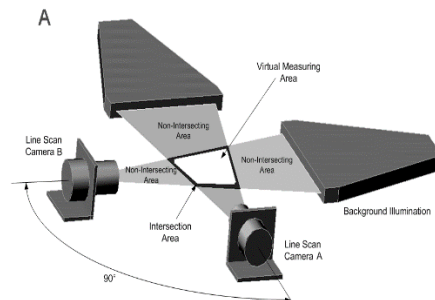


Figure 5a (top): 2DVD schematic diagram (from Schönhuber, 2008). 5b (bottom): 2DVD as installed at the Easton site.

The planes of the 2DVD line scan cameras are vertically separated by a calibrated distance of ~6.2 mm, allowing hydrometeor fall speeds to be calculated from the difference in the interruption times of the two beams. At the Easton site, the 2DVD and the MASC were horizontally separated by ~2 m. Both instruments were installed on platforms that raised the openings of their sampling areas to within ~0.25 m of the top of the surrounding wind screen (Fig. 5b).

The MASC sampling area is appreciable smaller than that of the 2DVD (~3 x 10 cm vs. 10 x 10 cm). Also, the restrictions imposed by the depth of field limits of the MASC cameras and spatial variations in the flash intensity cause many of the MASC images to have degraded focus and / or dim illumination. Despite these limitations, the MASC can provide detailed images of well-sampled snow particles. To develop a sense of the hydrometeor visualizations generated by the MASC and the 2DVD, the hollow plastic bead and the m4 machine screw shown in Figure 6 were dropped through both instruments.



Figure 6: Test objects dropped through the 2DVD and the MASC,

The 2DVD's orthogonal silhouette representations of these objects readily resolve the central opening in the bead (Fig. 7a). The finer scale threads on the machine screw are just visible (Fig. 7b).

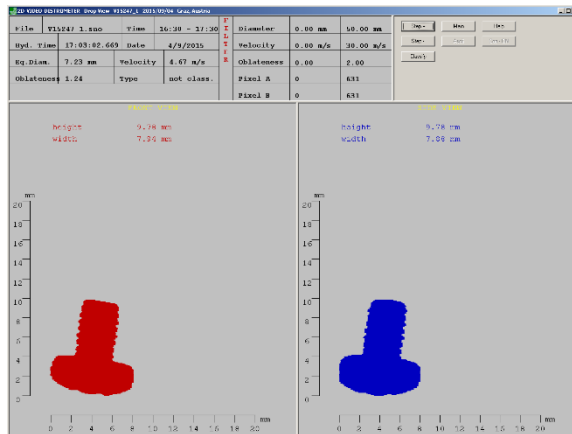
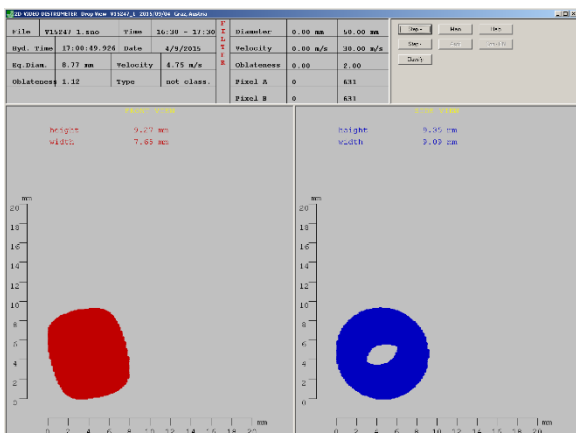


Figure 7: Orthogonal shadow views of the two test objects as recorded by the 2DVD.

The higher resolution MASC images reveal some more subtle physical attributes of these objects. For example, the slightly elevated seam around the "equator" of the bead and the rough quality of the start of the threading at the end of the screw can be seen (Fig. 8a and b).

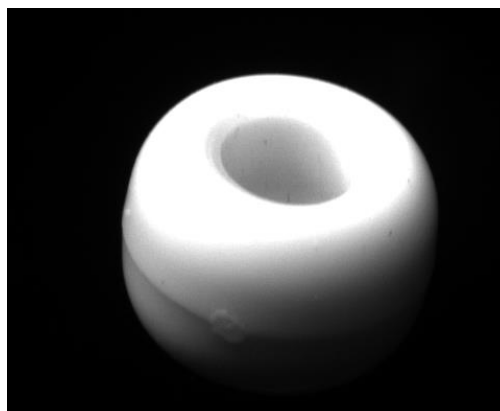


Figure 8: Plastic bead (8a) and machine screw (8b) images as recorded by the 5 Mpixel cameras in the MASC.

As noted in the introduction, a major goal of the MASCRAD project was the generation of 3D snow particle representations. Figure 9 shows an example 3D reconstruction based on the MASC images of the plastic bead. (The missing section on the right side of the bead is the result of a software problem that has been corrected).

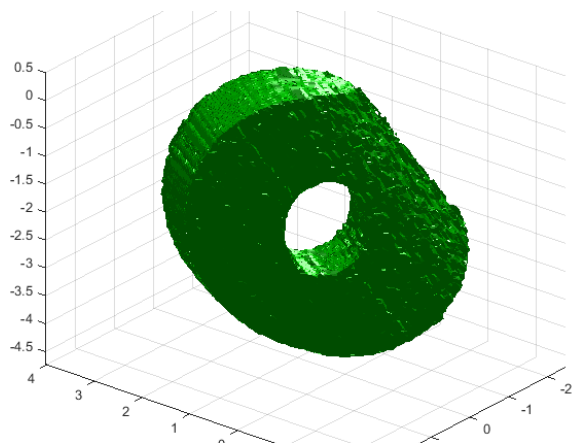


Figure 9: 3D reconstruction of the hollow plastic bead developed by applying the visual hull method to the images obtained using the MASC.

As of September, 2015, the development of 3D representations of snow particles was not possible when multiple hydrometeors were captured during a single MASC flash / camera system triggering event. Software improvements are underway to remove this restriction. As shown in Kleinkort et al. (2015), the currently available 3D particle reconstructions have been satisfactory for microwave backscattering calculations.

3. Example Cases

Using either individual or coordinated operations, the CSU-CHILL and NCAR S-Pol radars collected dual polarization data during essentially all significant snow events that occurred in the greater Easton Airport area between November, 2014 and April, 2015. The following three cases were selected to illustrate the diversity of hydrometeor image types that were collected with the MASC.

3.1 16 February 2015 negative Zdr graupel shower

MASCRAD project operations were conducted during the overnight hours of 15 – 16 February 2015 as a well-defined 500 mb upper trough system moved southward across the area. By sunrise on the 16th, skies were clearing as the area of light snowfall associated with the trough had moved well south of

Easton. The onset of surface heating coupled with lower tropospheric cold air advection suggested that steep lapse rates and convective clouds were likely to develop later in the day (Fig. 10a).

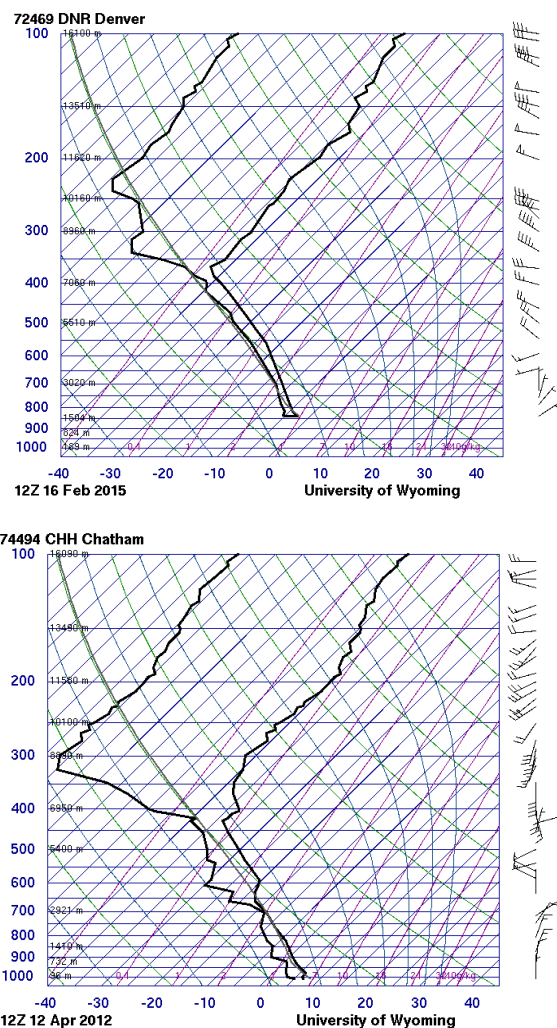


Figure 10: (a, top) Denver sounding data at 12 UTC on 16 February 2015. Graupel showers developed in the greater Easton area approximately 6 hours later. (b, bottom) Chatham, MA sounding associated with the graupel showers investigated in Evaristo et al. (2013).

The Denver 12 UTC 16 February 2015 sounding bore significant similarity to the environmental conditions under which graupel shower development was reported in Evaristo (2013; Fig 10b). In both soundings, moisture and instability were generally confined to heights below the 500 mb level with evidence of backing wind directions with increasing height (i.e., cold air advection) through much of the moist layer. In both cases, shallow convective showers developed as surface heating occurred later in the day.

An overview of the initial echo development as seen by the Denver / Front Range Airport (KFTG) NWS WSR-88D radar is shown in Figure 11.

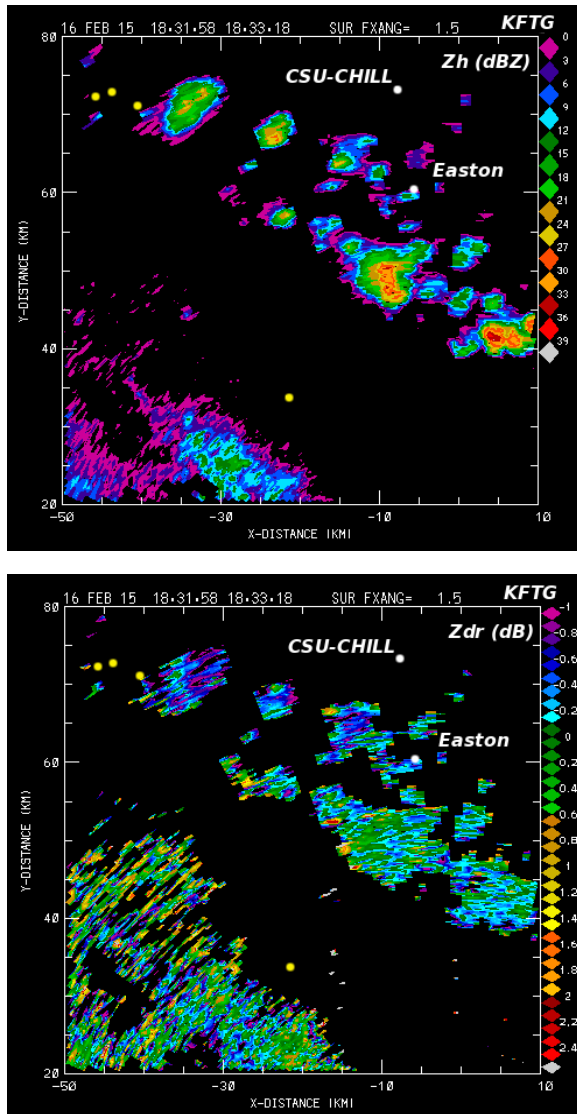


Figure 11: KFTG 1.5° elevation angle PPI data from 1831 UTC on 16 February 2015. (a, top) Horizontal reflectivity in dBZ. (b, bottom) Differential reflectivity in dB. Axes are distances from KFTG in km. Yellow dots mark locations where Community Collaborative Rain, Hail and Snow network (CoCoRaHS) volunteer observers reported graupel.

By 1831 UTC (1131 MST), small convective echoes with maximum core reflectivities of ~35 dBZ had formed along a line located just south of the Easton site (Fig. 11a). Fractionally negative Zdr values were consistently observed in these echo cores. These reflectivity and Zdr values are consistent with surface reports of small, conical graupel in the fall and spring seasons Evaristo (2013). The existence of graupel on

this date was confirmed by examining the observations filed by observers in the Community Collaborative Rain, Hail and Snow (CoCoRaHS) network. The yellow dots included in Figure 11 mark locations where these observers reported graupel during the 24 hours ending at 13 UTC on the 17th.

At 1824 UTC, the CSU-CHILL radar conducted several general surveillance observations before starting dedicated scanning over Easton. The aforementioned shower band is shown in Figure 12.

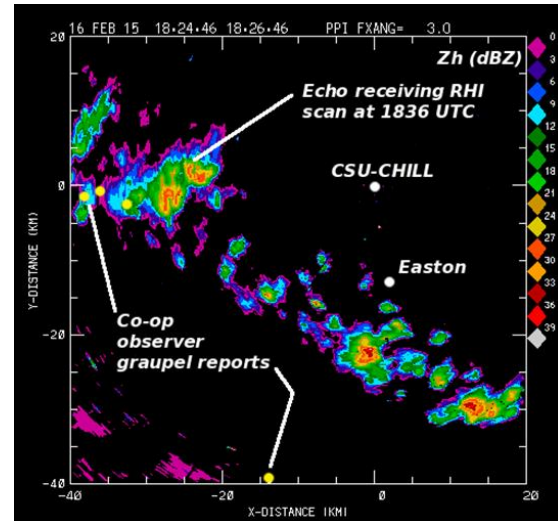


Figure 12: CSU-CHILL reflectivity data observed in a 3° PPI scan at 1825 UTC. Axes are in km distances from CSU-CHILL.

RHI scans were done through the echo complex located ~25 km west of the radar in Figure 12. The reflectivity and Zdr data in one of these RHI sweeps is shown in Figure 13.

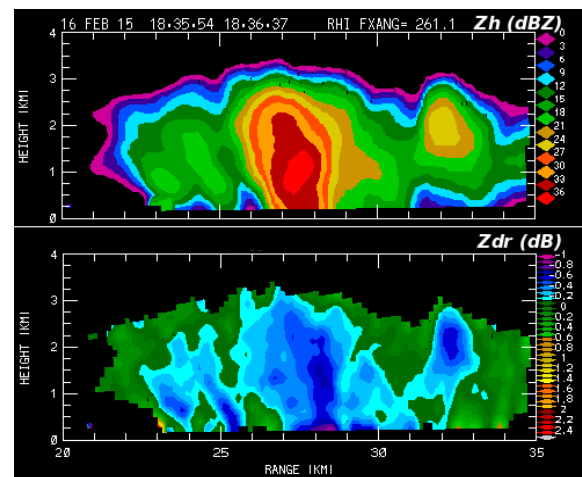


Figure 13: CSU-CHILL reflectivity (top) and Zdr (bottom) data in an RHI scan through a shower located near Loveland, Colorado on 16 Feb. 2015.

The RHI reveals that the convective echoes were shallow, with maximum tops on the order of 4 km AGL (5.4 km MSL). The vertical extent of the showers was limited to the depth of the moist, surface-based layer seen in Figure 10a. In a consistent pattern with the KFTG data, the CSU-CHILL observations confirm that negative Zdr values were associated with the higher reflectivity regions.

Additional showers began to develop near the Easton site at ~ 1840 UTC. CSU-CHILL scanning that repeated RHI's over the Easton site with a cycle time of ~2.25 minutes were started. The development and passage of several showers in close proximity to the Easton site was captured. Figure 14 shows a small sample of the echo evolution that was repeatedly observed during this intensive RHI period.

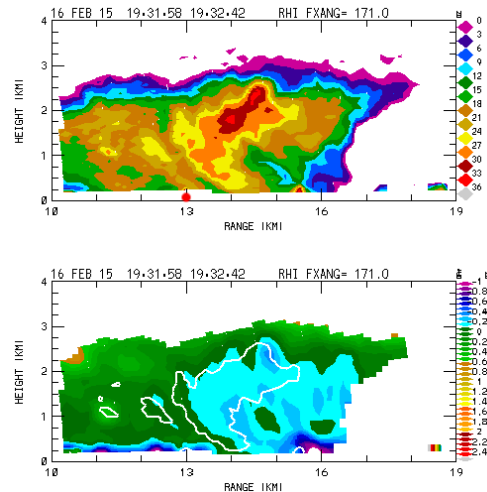
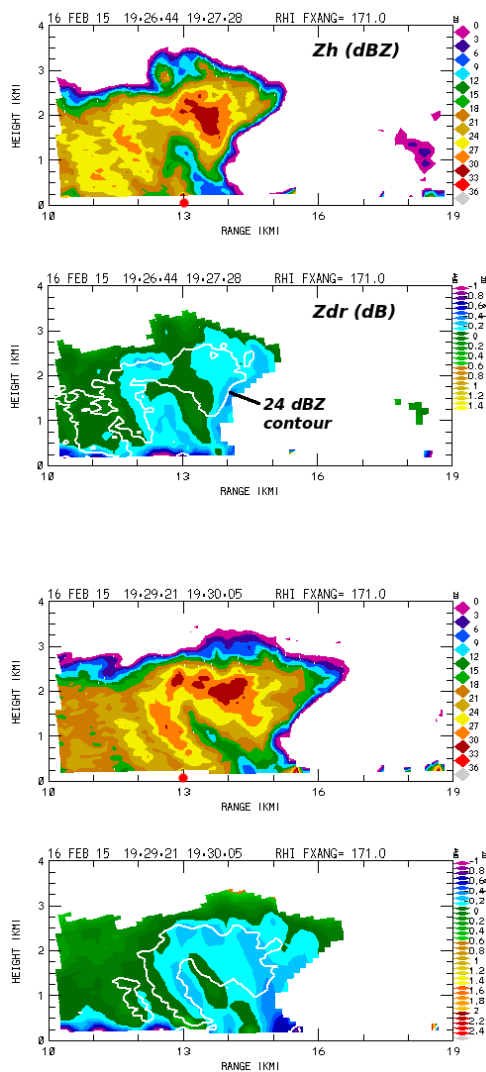


Figure 14: Time evolution of reflectivity and Zdr in a series of three successive CSU-CHILL RHI scans over the Easton site on 16 February 2015. The Easton site is marked by the red dot at the 13 km range point in the reflectivity frames.

The RHI data showed a repeated tendency for echo development to initially occur aloft in the ~2 – 3 km AGL height layer. These elevated echo cores then elongated downwards, reaching the surface within ~ 3 – 5 minutes. The majority of these developing / descending higher reflectivity cores were characterized by negative Zdr values on the order of -0.5 to -0.2 dB. The CSU-CHILL Zdr data calibration was checked using vertically-pointed data collected during a snow event six days later. Based on this vertically-pointed data, +0.2 dB was added to the values in the archive data files. This adjustment has been applied to the plots shown in Figure 14. The fractionally negative Zdr values are consistent with those observed by the NWS KFTG radar in this event.

Slightly negative Zdr values have been associated with graupel particles, especially when certain conical graupel shapes are present (Evaristo 2012, Liu and Chandrasekar, 2000, Straka et al., 2000).

The descending reflectivity cores observed on 16 February 2015 were never well-centered on the Easton site, as a result, the MASC only collected ~50 particle images during the ~1900 – 2015 UTC period. Within this small sample, lump type graupel particles were frequently observed (Fig.15).

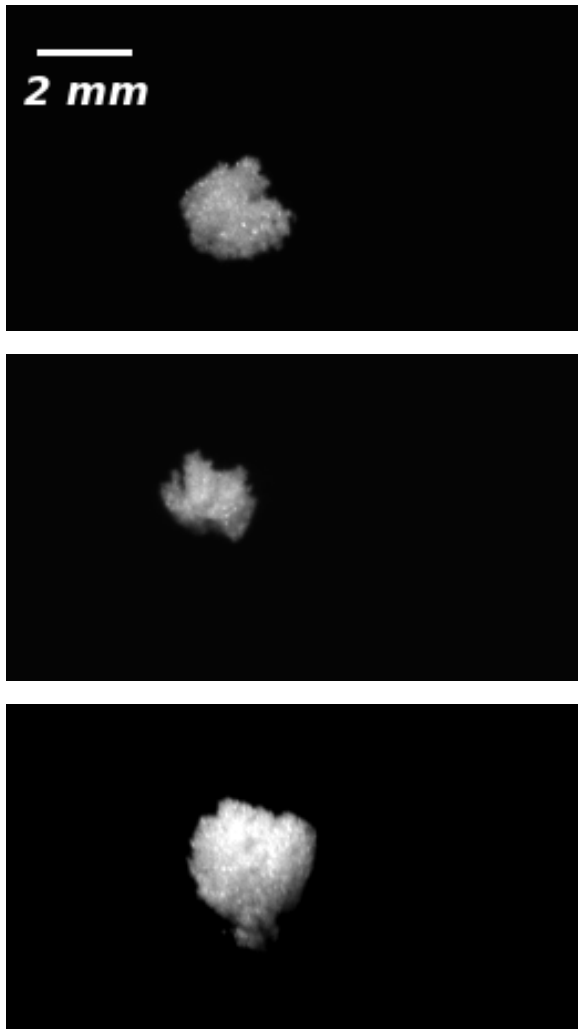


Figure 15: Example MASC images recorded during the 16 February 2015 graupel showers at the Easton site.

Additional confirmation that small graupel was a significant component of this shower activity is available in the post-event manual photograph taken at the Easton site at 2110 UTC (Fig. 16). This photograph was taken ~1 hour after the last of the convective echoes seen in the RHI scans had moved off to the south of Easton. The underlying snow patch was left by the preceding night's precipitation. The collection of ~2 – 4 mm graupel particles left on top of the snow was due to the multiple shower passages that occurred around mid-day on 16 February 2015. Scattering calculations based on the MASC and 2DVD images captured during this event are in progress. Preliminary results indicate the axis ratios of the graupel particles tended to become slightly prolate with increasing diameter. This shape characteristic in all probability accounts for the fractionally negative Zdr values that were observed (Bringi et al., 2015).



Figure 16: Example photograph of the graupel particles found at the Easton site after the convective echo passages recorded on 16 February 2015.

3.2 Heavy snow band on 21 February 2015 with near 0 dB Zdr in aggregated snow particles

The second MASCRAD project example case took place on 21 February 2015 when a major snow band associated with a cold frontal passage moved across the Easton site. Figure 17 shows the low-level reflectivity pattern observed by the S-Pol radar as the leading edge of this snow band was just reaching the CSU-CHILL site at 2051 UTC. The reflectivity values in excess of 30 dBZ were some of the highest levels observed from snow echoes during the field project.

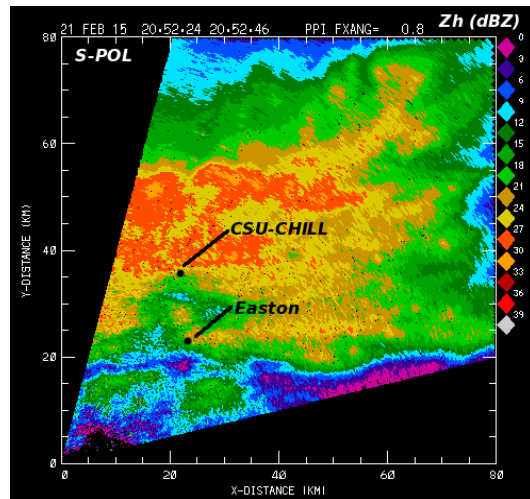


Figure 17: S-Pol reflectivity data collected in a 0.80 PPI scan as a major snow band arrived at the CSU-CHILL radar site at 2051 UTC on 21 February 2015. Axes are in km from S-Pol.

Figure 18 shows an RHI scan taken as the maximum reflectivity portion of the snow band was in the vicinity of the Easton site (range 13 km).

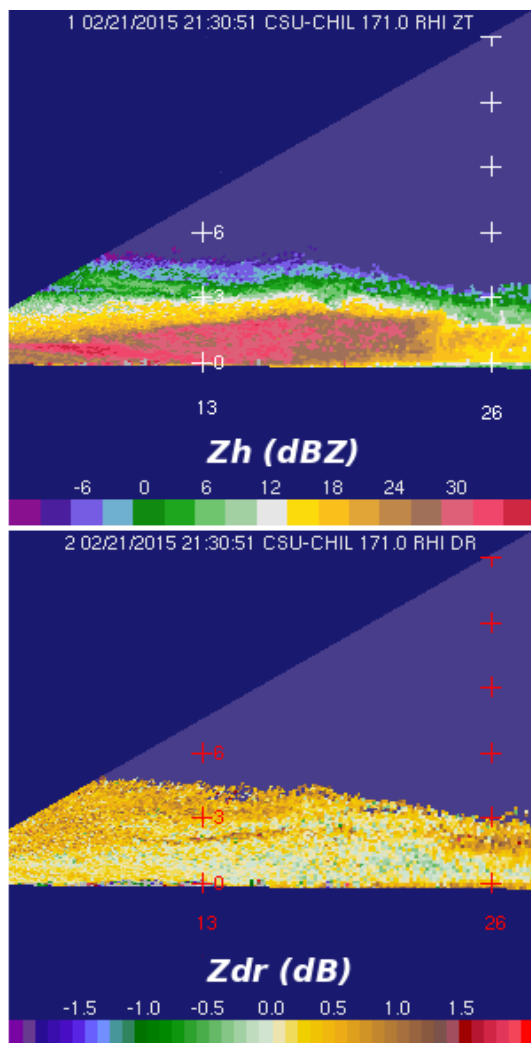


Figure 18: RHI scan over the Easton site (located at a range of 13 km) at ~2131 UTC on 21 February 2015. Maximum reflectivities slightly exceeded 30 dBZ (top panel). Differential reflectivities were near 0 dB in the high reflectivity regions.

Areas of light snow were fairly widespread before the surface cold front and primary snow band arrived in the Greeley area near 21 UTC. The arrival of the cold front brought northerly winds gusting to $\sim 15 \text{ ms}^{-1}$ and markedly reduced visibility in moderate – heavy snow at the CSU-CHILL site. The RHI data showed an echo depth increase of 1.5 – 2 km in association with the arrival of the snow band. Differential reflectivity was consistently near 0 dB in the lowest ~ 1 km in the higher reflectivity portions of the snow band.

Selected MASC images from this high reflectivity period are shown in Figure 19. Images containing

relatively large diameter particles with good focus and illumination were the selected. The larger diameter particles were of interest since they primarily influence the radar return signal.

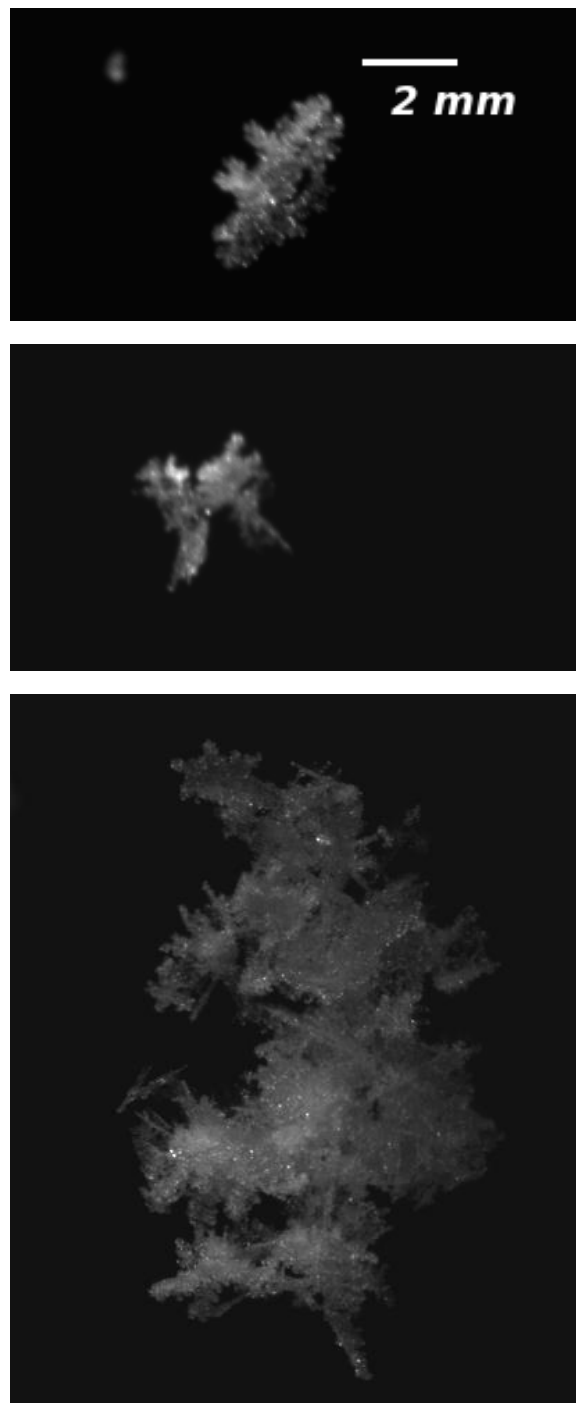


Figure 19: Selected MASC images starting at 2141 UTC on 21 February 2015.

The MASC images during the passage of the high reflectivity axis of the snow band were typically rimed

aggregates. Based on the MASC’s rapid flash rate, particle concentrations were high. The irregular shapes and orientations of these aggregates is consistent with the observed near 0 dB Zdr values.

A comparison of the Zdr values observed in the 16 February graupel showers and in the 21 February snow band is shown in Figure 20. Both events have a mode Zdr value that is very close to 0 dB. The 16 February case, which contained more lump graupel particles than aggregates, had a longer tail of values extending into the negative Zdr range.

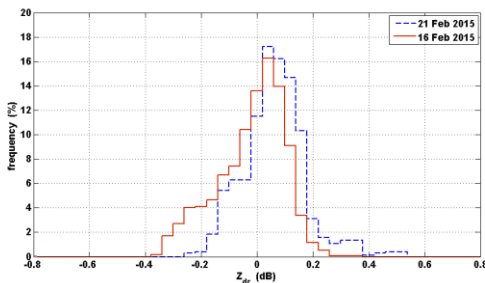


Figure 20: Zdr histograms for the 16 February graupel 21 February snow band cases.

Similar histograms for Linear Depolarization Ratio (LDR) are shown in Figure 21. The snow band case (blue trace) shows slightly higher depolarization levels. This is probably related to the more irregular / less spherical shapes of the large aggregates that were documented in the snow band.

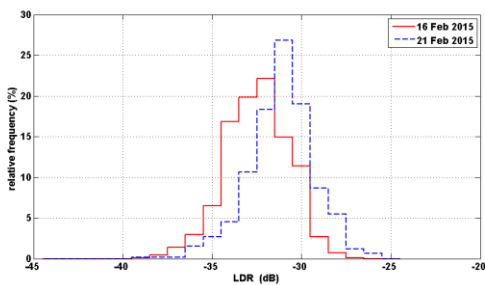


Figure 21: LDR histograms for the 16 February graupel 21 February snow band cases.

3.3 Positive Zdr “pristine crystal” snow on 3 March 2015.

In contrast to the two previous “active” cases in which local convection (16 February graupel showers) and well-organized frontal lifting (21 February snow band) were occurring, the final event took place as an area of light snow was fading in terms of horizontal extent and reflectivity. On the morning of 3 March 2015, an area of light to moderate snow had passed the Easton

site while moving from north to south. By ~1800 UTC, only a shallow (~1 km deep), low reflectivity (single digit positive Zh values) remained over the Easton site. Within this tenuous residual echo layer, Zdr values were distinctly positive, with isolated maximum values of ~ +5 dB (Fig. 22).

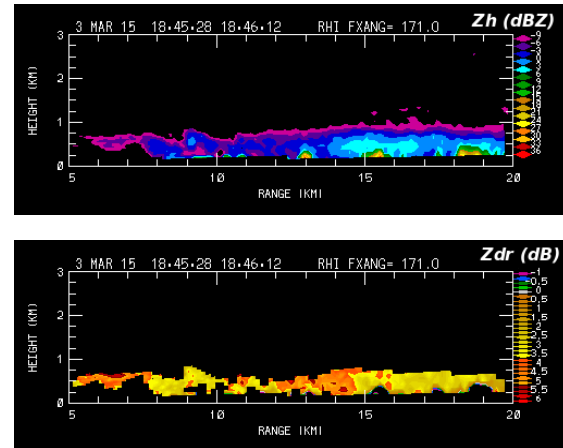


Figure 22: Reflectivity (top) and differential reflectivity (bottom) in an RHI scan over the Easton site at 1845 UTC on 3 March 2015.

Quantification of the reflectivity and Zdr values observed in this layer near Easton are shown in Figure 23.

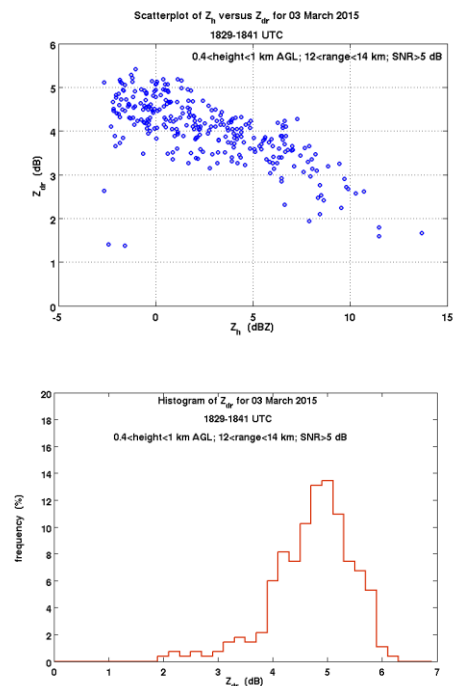


Figure 23: Zh vs. Zdr (top) and Zdr histogram (bottom) for 1829 – 1841 UTC on 3 March 2015 in the immediate Easton area.

This shallow, low reflectivity environment reduced the probabilities of particle riming and collisions. The selected MASC images shown in Figure 24 have more readily apparent individual crystal components vs. the heavily rimed aggregates seen in the snow band of 21 February.

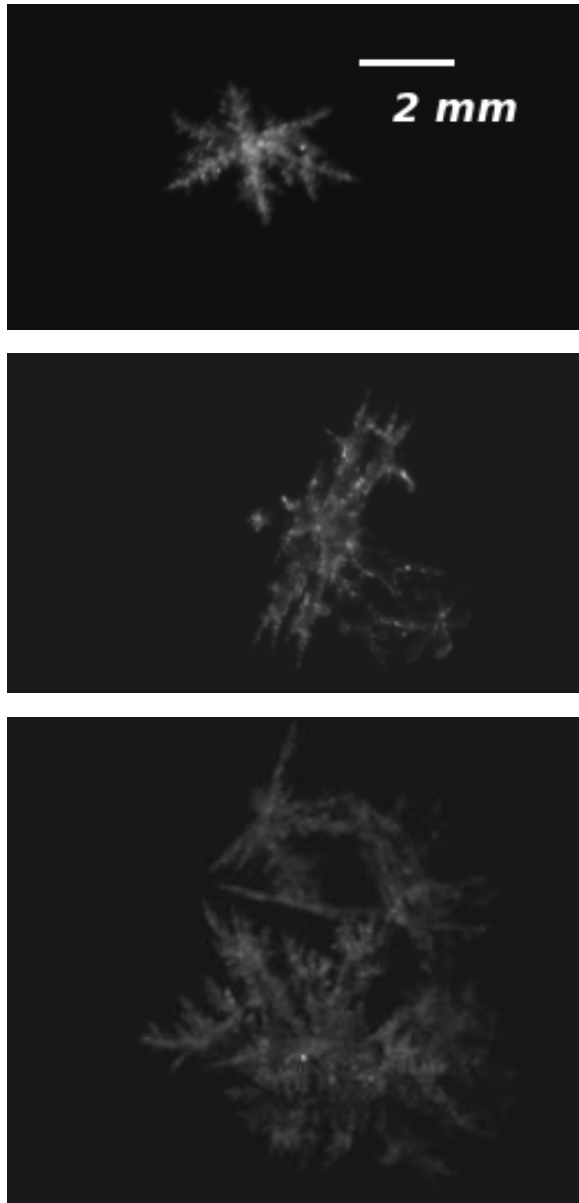


Figure 24: Selected MASC images between 1833 and 1838 UTC on 3 March 2015.

The more pristine, planar crystal forms on 3 March 2015 would be expected to fall in a maximum drag / quasi-horizontal orientation (Ono, 1969). This fall mode would produce the distinctly positive Z_{dr} 's that were observed in the CSU-CHILL data.

4. Conclusions

The initial season of MASCRAD project operations (November 2014 – April 2015) captured a variety of winter season precipitation events. The hydrometeor images collected by the MASC camera provided useful visual characterizations of several important physical characteristics (i.e., basic crystal habits, extent of aggregation and riming, etc.) Multiple MASC images also supported 3D snow particle reconstructions that provided usable input for advanced microwave scattering calculations. Software developments are currently underway to further automate the processing of the MASC image data and to process more complicated MASC scenes containing multiple particle images.

Acknowledgements:

NSF AGS-1344862 (MASCRAD)
NSF ATM-0735110 PPE9553 (CSU-CHILL)

References:

Bringi, V. N., B. Notaros, C. Kleinkort, G. J. Huang, M. Thurai, and P. Kennedy, 2015: Comprehensive analysis of an unusual winter graupel shower event observed by an S-band polarimetric radar and two optical imaging surface instruments. AMS 37th Conference on radar meteorology. Norman, OK September 13 – 18, 2015.

Chobanyan, E., N. J. Sekeljic, A. B. Manic, M. M. Ilic, V. N. Bringi, and B. Notaros, 2015: Efficient and accurate computational electromagnetics approach to precipitation particle scattering analysis based on higher-order method of moments integral equation modeling. *J. Atmos. Oceanic, Tech.*, 23, pp. 1745-1758.

Evaristo, R., T. Bals-Esholz, E. Williams, A.J. Fenn, M. Donovan, and D. Smalley, 2013: Relationship of graupel shape to differential reflectivity: Theory and observations. AMS 29th Conference on Environmental Information Processing, Austin, TX, January 6 – 10, 2013.

Garrett, T. J., C. Fallgatter, K. Shkurko, and D. Howlett, 2012: Fall speed measurement and high-resolution multi-angle photography of hydrometeors in free fall. *Atmospheric Measurement Techniques*, 5, pp. 2625-2633.

Kleinkort, C., G.J. Huang, S. Manic, P. Kennedy, J. Hubbert, A. Newman, V. N. Bringi, and B. Notaros, 2015: 3D shape reconstruction of snowflakes from multiple images, meshing, dielectric constant estimation, scattering analysis, and validation by

radar measurements. AMS 37th Conference on radar meteorology. Norman, OK September 13 – 18, 2015.

Liu, H., and V. Chandrasekar, 2000: Classification of hydrometeors based on polarimetric radar measurements: Development fuzzy logic and neuro-fuzzy systems, and in-situ verification. *J. Atmos. Oceanic Tech*, 17, pp. 140-164.

Ono, A., 1969: The shape and riming properties of ice crystals in natural clouds. *J. Atmos. Sci*, 26, pp. 138-147.

Schönhuber, M., G. Lammer, and W. L. Randeu, 2008: The 2D-video-distrometer. *Precipitation: Advances in Measurement, Estimation and Prediction*, S. Michaelides, Ed., Springer, 3–31, doi:10.1007/978-3-540-77655-0_1.

Straka, J. M., D. S. Zrnic, and A. V. Ryzhkov, 2000: Bulk hydrometeor classification and quantification using polarimetric radar data: Synthesis of relations. *J. Appl. Meteor*, 79, pp. 1347-1372.